Frequency-Domain PML Layer Based on the Complex Mapping of Space Boundary Condition Treatment

H. A. Jamid

***Abstract*—Mapping of real space into a complex one is done in order absorb the radiative field. The boundary condition which ensures reflectionless incidence at the vacuum/PML interface is established. The application of this boundary condition results in a modified finite-difference approximation of the second derivative of the field. This approach, which is valid only for frequency-domain methods is applied using the Method of Lines. Comparison of theory and numerical simulation establishes the validity of the approach.**

***Index Terms*—Finite-difference methods, method of lines, perfectly-matched layer.**

I. Introduction

THE recent interest in highly effective absorbers for terminating the computational window has been stimulated by Berenger's work [1]. This work is based on a non-Maxwellian approach in which the electromagnetic field is split prior to imposing appropriate conditions for reflectionless absorption. A Maxwellian version of the perfectly-matched layer (PML) was later introduced [2]. This approach relies on the introduction of a lossy uniaxial absorbing medium inside the PML. The uniaxial approach was later shown to be equivalent to Berenger's method [3]. Other PML implementations includes its modification to enhance the attenuation rate of evanescent modes [4] and also to terminate conductive media [5]. Though the initial applications of the PML have been made within the finite-difference time-domain (FDTD) modeling scheme, extension to the frequency-domain methods has also been made [6]–[10]. The particular feature of interest in this later work is the mapping of real space into a complex one in order to absorb the radiative field. The advantage of this approach is its conceptual simplicity and ease of implementation. It also does not demand material absorption in the PML, which makes it independent of field polarization and material properties.

If the PML region is made sufficiently wide, only negligible reflections at the extreme edges of the computational window may occur. However, significant numerical reflection may occur at the inner wall of the PML [9]. Assuming the computational window is positioned normal to the x-direction, the distance within it is mapped into the complex-domain and expressed as $\overline{x}(x) = \sigma_r(x) + i\sigma_i(x)$. Where $\overline{x}$ denotes the resulting complex space, $\sigma_r(x)$ and $\sigma_i(x)$ are the mapping functions from the real space x, into the real and imaginary parts of the complex space, respectively. Thus, inside the PML, the radiative field in the x-direction, $\exp(ik_x x)$ is mapped into $\exp[ik_x\sigma_r(x)]\exp[-k_x\sigma_i(x)]$, which appears to attenuate in the x-direction if the mapping function $\sigma_i(x) > 0$. It is our purpose here to establish the interface conditions that allow the application of sufficiently large values of loss within the PML, while satisfying the requirement of reflectionless incidence at the inner wall of the PML.

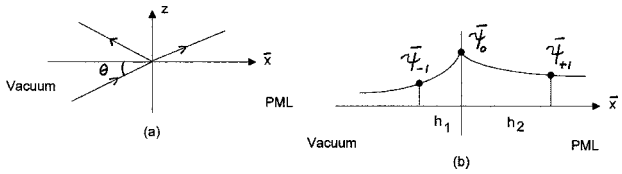

Fig. 1. (a) Plane wave incident from vacuum onto the PML. (b) Discretized field around the vacuum/PML interface.

II. Theory

First, we unify the description of space in both vacuum and the PML using the single variable $\overline{x}$, where $\overline{x}(x) = x$ in vacuum (self mapping) and $\overline{x}(x) = \sigma_r(x) + i\sigma_i(x)$ in the PML. The time-harmonic electromagnetic field $\psi(x, y, z)$, is then mapped into $\overline{\psi}(\overline{x}, y, z)$ by replacing x by $\overline{x}$ throughout the problem space. Thus, the field in vacuum remains unchanged due to this mapping (i.e., $\overline{\psi} = \psi$). However, inside the PML, $\overline{\psi} \neq \psi$.

Assuming a radiative field is incident from vacuum onto the PML as shown in Fig. 1(a). The incident, reflected and transmitted fields can be described by a discrete superposition of plane waves. Without loss of generality, we will only consider the x-variation of the field in the discussion to follow. Assuming $e^{-k\omega t}$ variation, the mapped field $\overline{\psi}(\overline{x})$ in vacuum and in the PML is respectively given by

$$\overline{\psi}(\overline{x}) = \sum_n a_n e^{ik_{xn}\overline{x}} + \sum_n r_n a_n e^{-ik_{xn}\overline{x}}, \qquad \overline{x} \leq 0 \quad (1)$$

$$\overline{\psi}(\overline{x}) = \sum_n t_n a_n e^{ik_{xn}\overline{x}}, \qquad \overline{x} \geq 0 \quad (2)$$

where k_{xn} is the x-component of the wave vector associated with the nth plane wave, a_n, r_n, and t_n are respectively, the amplitude, the reflection and transmission coefficients of the nth incident plane wave. Because no material discontinuity is present in this case, k_{xn} retains the same value in both regions.

Manuscript received May 15, 2000; revised July 5, 2000. This work was supported by King Fahd University of Petroleum and Minerals.

The author is with the Electrical Engineering Department, King Fahd University of Petroleum and Minerals, Dhaharan, Saudi Arabia (e-mail: hajamed@kfupm.edu.sa).

Publisher Item Identifier S 1051-8207(00)08794-8.

Using the above equations, we obtain, for each region, an expression for $\overline{\psi}^{(m)}$, the mth derivative of $\overline{\psi}$ with respect to $\overline{x}$. Imposing continuity of $\overline{\psi}^{(m)}$ at $\overline{x}=0$, we have

$$\sum_n a_n(k_{xn})^m[1+(-1)^m r_n] = \sum_n a_n(k_{xn})^m[1+r_n]. \quad (3)$$

The left-hand and the right-hand terms of the above equation represent $\overline{\psi}^{(m)}$ on the vacuum side and the PML side of the interface, respectively. In arriving at (3), the relationship: $t_n = r_n + 1$ has been used. Also, in arriving at (3), we have set $\overline{x}=0$ at the interface. This means that the mapping functions used in the PML should satisfy the condition: $\overline{x}(0) = \sigma_r(0) + i\sigma_i(0) = 0$. This condition demands the continuity of both mapping functions at the interface, or equivalently, continuity of $\overline{x}(x)$ at $x=0$. Equation (3) leads to the condition: $(-1)^m r_n = r_n$. If $r_n = 0$, this condition is satisfied for all values of m. Hence, $r_n = 0$ implies continuity of all $\overline{\psi}^{(m)}$. Thus, continuity of *all* $\overline{\psi}^{(m)}$ at $\overline{x}=0$ is a *necessary* condition for reflectionless incidence. For even values of m, the same condition is satisfied by arbitrary values of r_n and it does not impose any particular value on r_n. However, for any odd value of m, this condition requires $r_n = 0$. We thus conclude that continuity of *any* odd derivative of $\overline{\psi}$ at the inner wall of the PML is a *sufficient* condition for reflectionless incidence. This establishes the necessary and sufficient conditions for zero reflection at the vacuum/PML interface. These conditions are valid, whether the PML is lossy ($\sigma_i(x) > 0$) or lossless ($\sigma_i(x) = 0$). They only establish the requirements that guarantee reflectionless incidence when space is mapped in a *continuous* manner.

We next derive a finite-difference approximation to the second derivative of the field that takes into account the above conditions at the vacuum/PML interface. Fig. 1(b) shows the discretized field $\overline{\psi}$ around the vacuum/PML interface, assumed to be located at $\overline{x}=0$. Using Taylor series expansion of the field $\overline{\psi}$ in terms of $\overline{\psi}^{(m)}$:

$$\overline{\psi}_{-1} = \overline{\psi}_{\overline{0}} - h_1\overline{\psi}_{\overline{0}}^{(1)} + \frac{h_1^2}{2}\overline{\psi}_{\overline{0}}^{(2)} - \frac{h_1^3}{6}\overline{\psi}_{\overline{0}}^{(3)} + \frac{h_1^4}{24}\overline{\psi}_{\overline{0}}^{(4)} + \cdots \quad (4)$$

$$\overline{\psi}_{+1} = \overline{\psi}_{\substack{+\\0}} + h_2\overline{\psi}_{\substack{+\\0}}^{(1)} + \frac{h_2^2}{2}\overline{\psi}_{\substack{+\\0}}^{(2)} + \frac{h_2^3}{6}\overline{\psi}_{\substack{+\\0}}^{(3)} + \frac{h_2^4}{24}\overline{\psi}_{\substack{+\\0}}^{(4)} + \cdots \quad (5)$$

where the minus and plus signs refer to quantities in vacuum and in the PML, respectively. The parameters h_1 and h_2 represent the mesh size on the vacuum and the PML sides of the interface, respectively ($h_1 = \Delta\overline{x} = \Delta x$ and $h_2 = \Delta\overline{2} = \Delta\sigma_r + i\Delta\sigma_i$). For a lossy PML, $h_1 \neq h_2$, since h_1 is real and h_2 is complex. Obviously, there exits a discontinuity in the mesh size at the vacuum/PML interface when the PML is lossy. In order to achieve reflectionless incidence at the vacuum/PML interface, we impose the required conditions discussed above, by using $\overline{\psi}_{\substack{+\\0}}^{(m)} = \overline{\psi}_{\overline{0}}^{(m)} = \overline{\psi}_0^{(m)}$ in (4) and (5). Eliminating $\overline{\psi}_0^{(1)}$ from the resulting equations and ignoring terms higher than $\overline{\psi}_0^{(2)}$, we have

$$\overline{\psi}_0^{(2)} \simeq \frac{h_1\overline{\psi}_{+1} - (h_1+h_2)\overline{\psi}_0 + h_2\overline{\psi}_{-1}}{0.5h_1h_2(h_1+h_2)}. \quad (6)$$

Equation (6), represents the *required* finite-difference approximation of $\overline{\psi}_0^{(2)}$. When no mesh size discontinuity is present (i.e., $h_1 = h_2 = h$), (6) reduces to the well-known *central*-difference approximation of $\overline{\psi}_0^{(2)}$. Due to the approximate nature of (6), it satisfies the necessary conditions that require continuity of all $\overline{\psi}^{(m)}$ up to $m=2$ only, since higher order terms have been ignored. However, it satisfies one sufficient condition for reflectionless incidence, namely, continuity of $\overline{\psi}^{(1)}$. Thus, when implanting (6), some numerical reflection from the vacuum/PML interface is expected. The level of reflection is related to the truncation error in (6). There exists a number of ways to reduce these errors in order to improve the performance of the PML. This can be done for instance by a good choice of mapping functions or by increasing the order of the finite-difference approximation $\overline{\psi}_0^{(2)}$ of in (6), to account for higher order terms. In this work, we will consider only the linear mapping functions: $\sigma_r(x) = x$ and $\sigma_i(x) = \gamma x$. By varying the positive parameter γ, one can control the strength of absorption inside the PML. The complex space $\overline{x}$ in this case is given by $\overline{x} = x + i\gamma x$ and the mesh size h_2 takes the *uniform* value $h_2 = \Delta\overline{x} = \Delta x + i\gamma\Delta x$ throughout the PML.

The sum of the two leading error terms in (6) associated with the nth plane wave is given by

$$\delta = -\tfrac{1}{3}\gamma\Delta x k_{xn} + \tfrac{1}{12}[(\gamma^2-1) - i\gamma](\Delta x)^2 k_{xn}^2 \quad (7)$$

where δ has been normalized with respect to $\overline{\psi}_0^{(2)} = -k_{xn}^2\overline{\psi}_0$. The decay factor ξ within the PML for the nth plane is given by

$$\xi = e^{-\gamma\Delta x N k_{xn}} \quad (8)$$

where N is the total number of mesh points inside the PML. Equations (7) and (8) are useful in the design of the PML. The following discussion assumes that the PML will be used to absorb a wide range of $k_{xn} = k_0\cos\theta_n = (2\pi/\lambda)\cos\theta_n$ associated with the incident wave in order for the PML to have a broad-band feature. The angle θ_n of the nth incident plane is defined according to Fig. 1(a). The error δ has to be kept small to reduce reflection from the PML and ξ must also be kept small in order to prevent the decaying radiative waves within the PML from reaching the extreme walls of the problem space. If we insure that δ is small for the largest value of k_{xn} associated with the incident wave, namely $k_{x\,\max} = k_0$, then we insure that it is also small for all other values of k_{xn}. Thus in using (7), we replace k_{xn} by k_0, before error analysis is made. The parameter γ is then chosen such that the real parts of the two error terms in δ cancel each other. In this manner, the first leading error term in δ disappears. This value of γ is given approximately by

$$\gamma \simeq \frac{4}{\Delta x k_0}. \quad (9)$$

Consideration (8), however, is best done by first substituting the minimum value of k_{xn} of the incident wave, namely, $k_{x\,\min}$, because ξ has the largest value in this case. Assuming that $k_{x\,\min} \simeq 0.1k_0$, and that $\xi_{\max} = e^{-\gamma\Delta x k_{x\,\min} N} \simeq e^{-4}$, we have

$$N \simeq \frac{4}{\gamma\Delta x k_{x\,\min}} = \frac{40}{\gamma\Delta x k_0} = 10 \quad (10)$$

where (9) has been used to arrive at the above relation. It is important to note that in practice, (9) should be treated as an upper limit on the value of γ. Because, when is increased beyond this

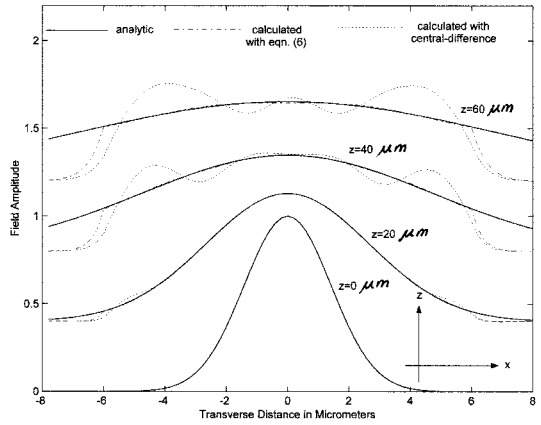

Fig. 2. Theoretical and calculated Gaussian beam propagation in vacuum.

value, the real part of the second error term starts to dominate δ and at some point δ becomes proportional to γ^2, leading to rapid growth both in the error and in the numerical reflection from the inner wall of the PML. Therefore, if very low reflection from the PML is required, γ should be reduced below the value suggested by (9) and in that case, N has to be *increased* accordingly.

III. Results and Discussion

The approach discussed above is potentially valid for all finite-difference frequency-domain methods based on the use of the second derivative of the field. The method of lines (MOL) [11], which fits into this category, has been chosen to demonstrate the validity of the present approach. Equation (6) can be incorporated into the MOL in a straight forward manner. As will be seen later, using (6) to approximate $\overline{\psi}^{(2)}$ at the vacuum/PML, very small reflection develop there. However, it will also be seen that when central-difference is used to approximate $\overline{\psi}^{(2)}$ at the inner wall of the PML, strong reflection occur there. The central-difference approximation of $\overline{\psi}^{(2)}$, does not account properly for the mesh size discontinuity present at the inner wall of the PML, and hence, it also does not satisfy the necessary or the sufficient conditions for zero reflection.

The propagation of a two-dimensional Gaussian beam in vacuum is simulated using the MOL. The Gaussian beam $\psi(x, z)$, which propagates in the z-direction, is placed in the center of the problem space and expressed as $\psi(x, z = 0) = \exp(-x^2/w^2)$ at the input plane $z = 0$. The spot size of the input Gaussian beam, $w = 2$ μm and the operating wavelength $\lambda = 1$ μm. Vacuum in this case occupies the region ($|x| < 6$ μm). Two identical PML layers are placed to the right and the left of the problem space occupying the regions $|x| > 6$ μm. Fig. 2 shows the theoretical and calculated Gaussian beam propagation. The beam progress is shown at $z = 0, 20, 40$, and 60 μm, respectively. The individual curves were shifted successively upwards by 0.4 for clarity. Two sets of calculated results are shown in Fig. 2. In one case (6) was used to approximate $\overline{\psi}^{(2)}$ at the vacuum/PML interface, and in the second case, central-difference approximation was used instead. Good agreement between the theoretical and calculated fields in vacuum is seen when (6) is used. However, strong reflections are seen to develop at the vacuum/PML interface, when the central-difference approximation is used. The above results were obtained using 60 points in the 12 μm wide vacuum, resulting in $\Delta x = 0.2$ μm. The other values used in this case are $\gamma = 3.2$ and $N = 10$ as suggested by (9) and (10), respectively. It is seen that the value of the loss parameter γ used in this case is relatively large, which results in a relatively small value of N. This value of γ causes a large discontinuity in the mesh size at the inner PML walls and this explains the reason for the failure of the central-difference approximation there. If the PML loss parameter γ is made very small ($h_2 = \Delta x + i\gamma\Delta x \simeq \Delta x = h_1$), the discontinuity in the mesh size is greatly reduced and the central-difference approximation may then be effectively used at the vacuum/PML interface. However, as suggested by (10), N has to be made large in this case, which results in a very inefficient implementation of the PML.

A similar argument to the above can be made for a PML having a graded loss profile. Numerical experiments done by the author show that for a PML having a graded loss profile, significant enhancement of the efficiency of the PML is seen when (6) is used in place of the central-difference approximation. Due to the limited space in this letter however, these results will not be presented here. Hence, using (6) instead of the central-difference approximation significantly enhances the efficiency of the PML implementation, whether the PML is uniform or graded in nature. This shows the importance of the present approach.

IV. Conclusions

For an efficient implementation of a reflectionless PML based on transforming real space into the complex domain, one must properly account for the resulting mesh size discontinuity in this case. This makes it possible to introduce a PML layer having a relatively large loss, while maintaining small reflection at the inner wall of the PML.

References

[1] J. P. Berenger, "A perfectly matched layer for the absorption of electromagnetic waves," *J. Comput. Phys.*, pp. 185–200, Oct. 1994.

[2] Z. S. Sacks, D. M. Kingsland, R. Lee, and J. F. Lee, "A perfectly matched anistropic absorber for use as an absorbing boundary condition," *IEEE Trans. Antennas Propagat.*, vol. 43, pp. 1460–1563, Dec. 1995.

[3] S. D. Gedney, "An anistropic perfectly matched layer-absorbing medium for termination of FDTD lattices," *IEEE Trans. Antennas Propagat.*, vol. 44, pp. 1630–1639, 1996.

[4] B. Chen, D. G. Fang, and B. H. Zhou, "Modified Berenger PML absorbing boundary condition for FD-TD meshes," *IEEE Microwave Guided Wave Lett.*, vol. 5, pp. 399–401, Nov. 1995.

[5] Y. H. Chen, W. C. Chew, and M. L. Oristaglio, "Application of perfectly matched layer for transient modeling of subsurface EM problems," *Geophysics*, vol. 62, pp. 1730–1736, Nov./Dec. 1997.

[6] W. C. Chew and W. H. Weedon, "A 3-D perfectly matched medium from modified Maxwell's equations with stretched coordinates," *Microwave Opt. Technol. Lett.*, vol. 7, no. 13, pp. 599–604, Sept. 1994.

[7] C. M. Rappaport, "Perfectly matched absorbing boundary conditions based on anistropic lossy mapping of space," *IEEE Microwave Guided Wave Lett.*, vol. 5, pp. 90–92, Mar. 1995.

[8] R. Mittra and U. Pekel, "A new look at the perfectly matched layer (PML) concepts for the reflectionless absorption of electromagnetic waves," *IEEE Microwave Guided Wave Lett.*, vol. 5, pp. 84–86, 1995.

[9] W. C. Chew and J. M. Jin, "Perfectly matched layers in the discretized space: an analysis and optimization," *Electromagnetics*, vol. 16, no. 4, pp. 325–340, 1996.

[10] S. J. Al-Bader and H. A. Jamid, "Perfectly matched layer absorbing boundary conditions for the Method of Lines modeling scheme," *IEEE Microwave Guided Wave Lett.*, vol. 8, pp. 357–359, Nov. 1998.

[11] R. Pregla and E. Ahlers, "The method of lines for the analysis of discontinuities in optical waveguides," *Electron. Lett.*, vol. 29, no. 21, pp. 1845–1847, Oct. 1993.